Biogeosciences Discuss., 9, 1237–1257, 2012
www.biogeosciences-discuss.net/9/1237/2012/
doi:10.5194/bgd-9-1237-2012

Biogeosciences Discussions

Scaled biotic disruption during early Eocene global warming events

S. J. Gibbs[1], P. R. Bown[2], B. H. Murphy[3], A. Sluijs[4], K. M. Edgar[1,*], H. Pälike[1], C. T. Bolton[5], and J. C. Zachos[3]

[1]Ocean and Earth Sciences, National Oceanography Centre Southampton, University of Southampton, European Way, Southampton, SO14 3ZH, UK
[2]Department of Earth Sciences, University College London, Gower Street, London WC1E 6BT, UK
[3]Department of Earth and Planetary Sciences, University of California, Santa Cruz, CA 95064, USA
[4]Biomarine Sciences, Institute of Environmental Biology, Utrecht University, Laboratory of Palaeobotany and Palynology, Budapestlaan 4, 3584CD, Utrecht, The Netherlands
[5]Departamento de Geologia, Universidad de Oviedo, Arias de Velasco, 33005 Oviedo, Asturias, Spain
[*]now at: School of Earth and Ocean Sciences, Cardiff University, Main Building, Park Place, CF10 3AT, Cardiff, UK

Received: 9 January 2012 – Accepted: 12 January 2012 – Published: 30 January 2012

Correspondence to: S. J. Gibbs (sxg@noc.soton.ac.uk)

Published by Copernicus Publications on behalf of the European Geosciences Union.

Abstract

Late Paleocene and early Eocene hyperthermals are transient global warming events associated with massive carbon injection or carbon redistribution in the ocean-atmosphere system, and are considered partial analogues for current anthropogenic climate change. Because the magnitude of carbon release varied between the events, they are natural experiments ideal for exploring the relationship between carbon cycle perturbations, climate change and biotic response. Here we quantify marine biotic variability through three million years of the early Eocene, including five hyperthermals, utilizing a method that allows us to integrate the records of different plankton groups through scenarios ranging from background to major extinction events. Our long-time-series calcareous nannoplankton record indicates a scaling of biotic disruption to climate change associated with the amount of carbon released during the various hyperthermals. Critically, only the three largest hyperthermals, the Paleocene Eocene Thermal Maximum (PETM), Eocene Thermal Maximum 2 (ETM2) and the I1 event, show above-background variance, suggesting that the magnitude of carbon input and associated climate change needs to surpass a threshold value to cause significant biotic disruption.

1 Introduction

Late Paleocene through early Eocene hyperthermals occurred against a backdrop of long-term climate warming between ~60 and ~50 million yr ago (Ma) (e.g., Cramer et al., 2003; Lourens et al., 2005; Quillévéré et al., 2008; Zachos et al., 2010). All are characterized by negative carbon isotope excursions (CIE) and deep-sea carbonate dissolution (Lourens et al., 2005; Zachos et al., 2005), indicating the release and/or redistribution of massive amounts of ^{13}C-depleted carbon between carbon reservoirs (e.g., Cramer et al., 2003; Lourens et al., 2005; Sexton et al., 2011). The PETM (~56 Ma) was the largest and most abrupt of these hyperthermals with a marine CIE of

BGD
9, 1237–1257, 2012

2.5–4.0 ‰, and was associated with lysocline shoaling of more than two kilometers and global warming of 5 to 8 °C (see Sluijs et al., 2007a; Zachos et al., 2005). This climate event was accompanied by dramatic biotic changes, including migration of terrestrial mammals, extinction of benthic foraminifera and a global expansion of tropical plankton (see Sluijs et al., 2007a; McInerney and Wing, 2011). ETM2 or H1 (~54 Ma) was the second largest hyperthermal, with a CIE of ~1.5 ‰ and ~3 °C warming (Lourens et al., 2005, Sluijs et al., 2009; Stap et al., 2010). Approximately 100 kiloyears (kyr) later, the H2 event occurred with a CIE of ~0.8 ‰ and warming of ~2 °C (Stap et al., 2010). The relationship between magnitude of the CIEs and degree of inferred warming are comparable, at least regionally, for the PETM, ETM2 and H2 events, suggesting that the isotopic composition and release mechanism of the injected carbon was similar across these events (Stap et al., 2010). These closely spaced, but varying magnitude CIEs/climate change events, provide enormous potential for quantifying biological sensitivity to carbon cycle perturbations. As new biotic records of these hyperthermals emerge, techniques are required that enable consistent and quantitative assessment of magnitudes and significance of biotic change in multi-taxic datasets. Here, we apply a modified coefficients of variation technique for quantifying levels of variation to a long time-series record of calcareous nannoplankton abundance across multiple hyperthermals, comparing results with other plankton groups and with the mass extinction at the Cretaceous-Paleogene boundary.

2 Material and nannofossil data

We generated high-resolution calcareous nannoplankton (nannofossil) assemblage records across a nine meter section at Ocean Drilling Program (ODP) Site 1209 (32°39.11′ N, 158°30.36′ E, present day water depth 2387 m) in the paleo-subequatorial Pacific Ocean (Fig. 1). This section spans five CIEs, the PETM, ETM2, H2, I1 and I2 (nomenclature following Cramer et al., 2003, and Zachos et al., 2010; Figs. 1 and 2), from ~53.0 to ~56.2 Ma. The CIEs are recognized in the isotopic composition of bulk

BGD
9, 1237–1257, 2012

sediment carbonate (Murphy et al., 2006) and typically correspond with clay-rich dissolution horizons, illustrated by the magnetic susceptibility record (Fig. 2b). The lysocline is not thought to have risen to the depth of this site during this interval and dissolution at this site was correspondingly less severe than, for example, the deep sites of the Walvis Ridge transect (Zachos et al., 2005). The age model for Site 1209 uses tie-points in the $\delta^{13}C$ record to correlate with the orbitally tuned stratigraphy and absolute ages of ODP Site 1262, summarized in Zachos et al. (2010) (Fig. 2a).

Assemblage data (% abundances) are based on statistically significant abundance counts of ~600–800 nannofossils per sample (Gibbs et al., 2006a), and were collected at 4–5 cm (~13 kyr) spacing. Initial species-level counts were performed on samples taken across the ETM2, supplementing data for the PETM (Gibbs et al., 2006a). Species were grouped into genera and ranked according to average abundances, with >97 % of the assemblage typically represented by around 10 genera. To facilitate relatively rapid data capture, generic counting was adopted, selecting genera that include the ten most abundant across the PETM and the ETM2, together 11 genera (Fig. 1).

3 Analytical approach and sensitivity tests

3.1 Combined smoothing and variance techniques

Our approach to quantifying and comparing biotic variability across hyperthermals required, (1) a means of utilizing routinely collected relative abundance data, (2) a technique ideally independent of taxic composition (which may vary with time and space due to evolution and biogeography, as well as between specialists), (3) a means to objectively quantify overall assemblage variability but remove dominance-biasing by a small number of taxa, and, (4) the application of an objective means to maximize signal-to-noise. These requirements are met by combining a method of generating the best-smoothed fit (Significant Zero crossings of derivatives, SiZer, Chaudhuri and Marron,

BGD
9, 1237–1257, 2012

1999), followed by a quantitative assessment of assemblage variability (summed coefficients of variation, Σ_{cv}).

First, each taxon's downcore record of relative abundance data was individually run through the SiZer program to produce a smoothed record (Fig. 1) that shows the least degradation but highest confidence in signal. The SiZer technique generates a set of smoothed curves, which use the full range of bandwidths available, and provides criteria by which the most appropriate of these smoothed curves can be chosen (Chaudhuri and Marron, 1999; Chaudhuri et al., 2012; Wagner, 2009; see the application to palaeoceanographic records in Rohling and Palike, 2005). Smoothing removes part of the noise inherent to these types of data and by using SiZer we introduce a transferable, objective set of criteria by which to increase the signal to noise ratio. The records of Σ_{cv} resulting from the SiZer smoothed abundances show similar trends to, but are consistently around half the amplitude of, the Σ_{cv} resulting from raw relative abundances (Fig. 3a).

Second, we calculated and summed the coefficients of variation (Σ_{cv}) for the most abundant taxa across moving windows. We used windows of 150 kyr, to capture the majority of each CIE (Figs. 2c and 4a), and 25 kyr, the shortest achievable with the sampling resolution of the data, to resolve patterns within each CIE (Fig. 4b). Because we want to directly compare net assemblage change across each event, we also calculated coefficients of variation (CV) across only the duration of each of the CIEs that are shorter than 150 kyr (Figs. 2c and 4a). CVs are calculated by determining the standard deviation of taxon abundance over a given stratigraphic interval followed by division by the taxon's mean abundance (Eq. 1, Fig. 3a and b). This provides a normalised measure of the spread of data about the arithmetic mean. Dividing the standard deviation by the average abundance is necessary in order to remove bias towards high abundance taxa. Higher abundance taxa can have a disproportionately large standard deviation, but equally, rare taxa that, for example, fluctuate between absence and rare occurrence would have a large standard deviation when divided by their average low abundance. Therefore the method excludes CVs from rare taxa (<0.7 %). For

BGD
9, 1237–1257, 2012

the Site 1209 record the number of taxa that qualifies is 11 and these taxa combined contribute >97 % of the assemblage. Herein, we have summed the CVs for the most common taxa to gain a quantified estimate of overall assemblage variance (Eq. 1).

$$\sum_{n=1:11}\left(\frac{\mathrm{SD}_{n,t_1\rightarrow t_2}}{\mathrm{mean}_{n,t_1\rightarrow t_2}}\right) \quad (1)$$

with t_1, t_2 being the start and end of the window, n the taxa number. In order to explore the influence of each taxon on the downcore record of Σ_{cv}, we recalculated the Σ_{cv} values multiple times, each time removing a different taxon (Fig. 2d). We can see that in this case three key taxa dominate in different portions of the record, *Coronocyclus*, *Zygrhablithus* and *Fasciculithus*. For example, *Fasciculithus* dominates the PETM Σ_{cv} values, which is not unreasonable given that the abundance and diversity loss of this genus is one of the characteristic features of this event. Therefore, the combination of multiple taxa ensures that we have an integrated picture of assemblage change through a dataset where variance occurs in different taxa at different stratigraphic levels.

We have also applied the Σ_{cv} technique to other published PETM datasets, including planktic foraminiferal and dinoflagellate cyst records (see Fig. 5a caption), choosing records with the necessary resolution, at least ~20 kyr sampling interval, to allow for a reasonable comparison of data. We used a window size corresponding to the total duration of the PETM, and have plotted in Fig. 5a peak and background values. Note that for the Bass River datasets, the resultant Σ_{cv} values may be an underestimate as the full duration of the CIE is not recorded. In addition, we applied the method to two sections that include the Cretaceous-Paleogene boundary (K-Pg, ~65 Ma), from ODP Sites 1210 and 1262 (Bown, 2005; Bernaola and Monechi, 2007), to provide comparison with the nearest mass extinction event (Fig. 5b). Again, for the K-Pg interval, for direct quantitative comparison, we used the top 11 most abundant nannofossil taxa, including both outgoing Cretaceous and incoming Paleocene taxa but excluding any obvious reworking of Cretaceous taxa in Paleocene sediments.

BGD
9, 1237–1257, 2012

3.2 Sensitivity tests and controls on the summed coefficients of variation record

The magnitude of CVs will be a function of sample window, which, ideally, is kept constant. In the present case, there will be some variation in window duration resulting from changes in sedimentation rates occurring at a resolution lower than the applied age model. Therefore, any resultant biases on the downcore Σ_{cv} record need to be taken into account when interpreting the records. We have tested the sensitivity of Σ_{cv} values by exploring the impact of varying window size and by artificially introducing hiatuses and dissolution. These tests have been applied to the depth record so we can see how any changes in sedimentation rate may be controlling the signal in the age-domain data. First, we calculated Σ_{cv} using different window durations from 10 cm up to 150 cm (Fig. 3c). As expected, Σ_{cv} values are higher when a larger depth window is applied because greater stratigraphic duration is being incorporated into each window, equivalent to decreasing sedimentation rate (Fig. 3c). To achieve an above background Σ_{cv} peak (equivalent to a value of around 1.6 Σ_{cv}, see Fig. 4a), requires a window size increase to just over 100 cm, equivalent to a minimum sedimentation rate reduction of approximately 55 % or an hiatus of just over 50 cm.

In the second sensitivity test, we introduced artificial hiatuses and dissolution, into one interval that has background variability and one that includes a CIE (Fig. 3d and e). Where the hiatus is introduced into a background interval we see elevated Σ_{cv} values, but not event-level values, and the longer the hiatus then the greater the apparent increase in Σ_{cv} (Fig. 3d). Where a hiatus was inserted at a CIE there is little change in the size of Σ_{cv}, but some impact on the structure of the record.

For the dissolution test, we removed 75 % of the nannofossils according to their different dissolution susceptibilities (following Gibbs et al., 2010). For example, we removed fewer discoasters (which are large and robust nannoliths) than we did *Campylosphaera* (a less robust coccolith). The resulting Σ_{cv} record suggests very little impact on the background assemblages but some amplification of the Σ_{cv} signal across the CIE (Fig. 3e). This is because the assemblages at this site in the background intervals

BGD
9, 1237–1257, 2012

are dominated by taxa that have very similar dissolution susceptibilities and so altering their abundances does not result in a major change in their recalculated relative abundances. In contrast, across the CIE intervals, there is a greater contribution by, for example, *Zygrhablithus*, discoasters and calcispheres, which increases the range of dissolution susceptibility in the observed dominant taxa. However, the change in Σ_{cv} is relatively small. Therefore, to produce the levels of Σ_{cv} associated with the PETM and ETM2 would require substantially larger hiatuses, dissolution or sedimentation rate changes than those introduced tested here. Such large sedimentological changes are usually apparent in these deep sea sediments and we are confident that this does not account for the larger Σ_{cv} peaks present. However, variability in the background record of Σ_{cv} may point to potential hiatuses/unconformities or sedimentation rate changes that are at a resolution higher than the age model, such as the unexplained variability at ~700 kyr above the PETM onset (Fig. 2c).

Finally, by looking at the ranked abundance of taxa from one time interval to the next we can test whether the fluctuations of dominant taxa are affecting the relative abundance of all the other taxa, for example, the fluctuations of *Zygrhablithus*. If only *Zygrhablithus* is changing, then the relative rank of all other taxa should not change. In fact the rank order in the non-*Zygrhablithus* taxa does change for both the PETM and the ETM2 but it did not for the I1. It could be, therefore, that the *Zygrhablithus* peak is the only major assemblage shift associated with I1 but this does not account for the assemblage shift across the PETM and ETM2.

4 Results and discussion

4.1 ODP Site 1209 hyperthermal record

The majority of values from the Site 1209 Σ_{cv} record (Fig. 2c) cluster between 0.4 and 1.6 Σ_{cv} (Fig. 4a), supporting the concept of a background range of biotic variability. However, several intervals have values outside this range, indicating a magnitude of variability that is exceptional or above-background biotic change, and supporting the

BGD
9, 1237–1257, 2012

existence of distinct "events". The highest Σ_{cv} value is associated with the PETM and there is a broadly linear trend of declining Σ_{cv} with decreasing size of CIE (Figs. 2c and 4a) for ETM2, I1 and H2, indicating a scaling of biotic response, which parallels the recent documentation of scaled temperature change and CIEs (Stap et al., 2010). The I2 CIE interval is less clear-cut, as it has an above background Σ_{cv} value if considered within a 150 kyr window, but not above background if using only the CIE duration (Fig. 2c). Similarly, H2 does not show anomalous values of Σ_{cv}. This indicates a biotic sensitivity threshold for calcareous nannoplankton for this location that lies between the CIEs of H2 and I1, at approximately 0.6 ‰.

Given that carbonate dissolution is associated with each of the CIEs, the scaling between event magnitude and biotic variance might reflect a simple relationship between carbonate erosion and dissolution-skewed abundance patterns. However, peak dissolution at each event is decoupled from abundance changes (Fig. 6) and the interval of dissolution is shorter than the window across which we calculate summed standard deviation. Therefore, it is unlikely that Σ_{cv} is wholly an artifact of co-varying dissolution with $\delta^{13}C$, although, based on the sensitivity tests, there is some potential for the Σ_{cv}–$\delta^{13}C$ relationship to be amplified.

When applied at higher stratigraphic resolution, the Σ_{cv} metric reveals important details of the timing of the environmental *versus* biotic perturbation (Fig. 2b). The PETM, ETM2, and I1 all show elevated Σ_{cv} values in the intervals immediately prior to the CIE onset, and each have recovery intervals in which Σ_{cv} values drop back to background levels before the carbon isotope values, a pattern also observed in temperature and $CaCO_3$ records (Zachos et al., 2003, 2005). This asymmetric structure appears to be a real feature of these events, rather than a data artifact, as it is seen in the original abundance data (Fig. 1). The shifts in nannoplankton assemblages prior to the respective CIEs are similar to abundance trends seen in PETM planktic foraminiferal and dinoflagellate cyst records from other locations (Thomas et al., 2002; Sluijs et al., 2007b), and our data suggests similar precursor environmental change also occurred prior to the ETM2 and I1 events.

BGD
9, 1237–1257, 2012

4.2 Global levels of variance

To test the wider significance of our analysis we have also analyzed published PETM plankton datasets from a range of shelf, slope and open-ocean localities in the Atlantic, Indian and Southern oceans, and included data for planktic foraminifera and organic-walled dinoflagellate cysts (Fig. 5a). The background to peak CIE Σ_{cv} values ($\Delta\Sigma_{cv}$) for nannoplankton from these other sites are comparable but with high latitude oceanic sites tending to exhibit higher levels of Σ_{cv}. The foraminifera and dinoflagellate data also return comparable ranges of variability (Fig. 5a), although consistently higher than the nannofossil records from the equivalent sites, perhaps suggesting slightly different relative sensitivities to environmental change in the different plankton groups. For example, dinoflagellate cyst abundance records across the PETM tend to exhibit characteristic "acmes". Multiple taxa appear and disappear, resulting in higher variance, as environmental thresholds are crossed across a range of environmental parameters including salinity, trophic state and water depth (e.g., Sluijs and Brinkhuis, 2009). In contrast, calcareous nannoplankton records tend to be dominated by a few species that may exhibit large abundance shifts but with the assemblage changes more typically represented by trends in the sub-ordinate taxa. These records demonstrate the potential of this approach for enabling integrated biotic comparisons and a means to holistically consider responses to coupled environmental changes, specifically the coupled warming, local nutrient and sea-level changes that account for the assemblage variations (see Sluijs et al., 2007a).

Finally, in order to place the hyperthermal nannoplankton perturbations in the broadest evolutionary context, we have also analysed data from the K-Pg mass extinction, ~65 Ma, which saw almost complete extermination of the group (Bown, 2005). The K-Pg scenario can be considered here as an end-member biotic perturbation, i.e. the pre-event assemblage has virtually no taxonomic similarity to the post-event assemblage. The K-Pg Σ_{cv} values from Shatsky Rise Site 1210 (for direct comparison with our hyperthermals dataset, Bown, 2005) and Walvis Ridge in the south Atlantic (Bernaola

BGD
9, 1237–1257, 2012

and Monechi, 2007), are 17 and 14, respectively (Fig. 5b), with a $\Delta\Sigma_{cv}$ of ~10–13. The Shatsky Rise Σ_{cv} of 17 appears close to the theoretical maximum for complete turnover at a single event level. This theoretical value can be estimated using different magnitudes of abundance changes across an event level, ranging from low-level to complete turnover in a highly heterogeneous assemblage (i.e. high disparity of abundance levels between taxa) to low-level to complete turnover in a more homogeneous assemblage. Higher theoretical values are possible but only when abundance declines are added prior to the event level turnover. The spectrum of Σ_{cv} resulting from the hyperthermals and the K-Pg analyses suggests sensitivity of the metric across the full environmental change spectrum. Therefore, whilst extinction rates data provide a quantitative means of characterizing biotic response to major events such as the K-Pg, the Σ_{cv} metric allows for sensitive characterization of biotic response to events, like the hyperthermals, where evolutionary turnover in plankton is relatively modest (Kelly et al., 1998; Gibbs et al., 2006b).

4.3 Threshold behaviour in plankton records

These Paleogene plankton data show threshold behavior and scaled response to environmental changes associated with carbon cycle perturbations. But is such behavior inherent in planktonic ecosystems and does this have any relevance for understanding how modern plankton might respond to future ocean change? Specifically our data show that nannoplankton assemblage perturbation occurs with environmental change associated with CIEs of above 0.6‰, equating to around 2°C of global warming using a proportional relationship between warming and CIE magnitude (Stap et al., 2010). This threshold value, however, may not be directly applicable in the modern ocean. First, carbon cycle rates of change are considerably faster at present and, second, the modern ocean has different physical baseline conditions (e.g., ocean-atmosphere chemistry and temperature; Zeebe et al., 2009; Goodwin et al., 2009; Ridgwell and Schmidt, 2010), with biological systems today adapted to icehouse climates, rather than the greenhouse climates of the Paleogene. On the one hand the modern ocean

BGD
9, 1237–1257, 2012

system may more rapidly reach the perturbation threshold because of the effects of increased rates of change in addition to the absolute levels of environmental change. By contrast, the greenhouse ocean system may already have been closer to a biologically-constrained upper thermal limit and so the threshold would have been reached through relatively smaller environmental changes (see discussion in Huber, 2008). Regardless of the absolute value, this estimate of thermal/carbon-perturbation threshold represents a first-order attempt to place constraints on biological thresholds with the possibility that future biotic response may scale in a similar way to the hyperthermals.

Acknowledgements. This research used samples provided by the Ocean Drilling Program. We acknowledge research fellowship funding to SJG by the Royal Society and the Natural Environment Research Council (NERC), BHM by a National Science Foundation grant (EAR-0120727 to JCZ), and AS by a Netherlands Organisation of Scientific Research (NWO-Veni grant 863.07.001. We thank Dyke Andreasen for his continued help in operating the UCSC Stable Isotope Lab. Thanks also to Mark Patzkowsky and Tim Bralower for advice and discussions and also to the authors cited for access to their published microfossil datas paper.

References

Bernaola, G. and Monechi, S.: Calcareous nannofossil extinction and survivorship across the Cretaceous-Paleogene boundary at Walvis Ridge (ODP Hole 1262C, South Atlantic Ocean), Palaeogeogr. Palaeocl., 255, 132–156, 2007.

Bown, P.: Selective calcareous nannoplankton survivorship at the Cretaceous-Tertiary boundary, Geology, 33, 653–656, 2005.

Bown, P. and Pearson, P.: Calcareous plankton evolution and the Paleocene/Eocene thermal maximum event: New evidence from Tanzania, Mar. Micropaleontol., 71, 60–70, 2009.

Bralower, T. J.: Evidence of surface water oligotrophy during the PETM: Nannofossil assemblage data from Ocean Drilling Program Site 690, Maud Rise, Weddell Sea, Paleoceanography, 17, 1023, doi:10.1029/2001PA000662, 2002.

Chaudhuri, P. and Marron, J. S.: SiZer for Exploration of Structures in Curves, J. Am. Stat. Assoc., 94, 807–823, 1999.

BGD

9, 1237–1257, 2012

Chaudhuri, P., Marron, J. S., Jiang, J. C., Kim, C. S., Li, R. Z., Rondonotti, V., de Uña Alvarez, J.: SiZer: which features are "really there"?, available at: http://www.unc.edu/~marron/DataAnalyses/SiZer_Intro.html, last access: January 2012.

Cramer, B. S., Wright, J. D., Kent, D. V., and Aubry, M.-P.: Orbital forcing of δ^{13}C excursions in the late Paleocene-early Eocene (chrons 24n–25n), Paleoceanography, 18, 1097, doi:10.1029/2003PA000909, 2003.

Gibbs, S. J., Bralower, T. J., Bown, P. R., Zachos, J. C., and Bybell, L.: Shelf and open-ocean calcareous phytoplankton assemblages across the Paleocene-Eocene Thermal Maximum: Implications for global productivity gradient, Geology, 34, 233–236, 2006a.

Gibbs, S. J., Bown, P. R., Sessa, J., Bralower, T. J., and Wilson, P. A.: Nannoplankton extinction and origination rates across the Paleocene-Eocene Thermal Maximum, Science, 314, 1770–1773, 2006b.

Gibbs, S. J., Stoll, H., Bown, P. R., and Bralower, T. J.: Ocean acidification and surface water carbonate production across the Paleocene-Eocene Thermal Maximum, Earth Planet. Sc. Lett., 295, 583–592, 2010.

Goodwin, P., Williams, R. G., Ridgwell, A., and Follows, M. J.: Climate sensitivity to the carbon cycle modulated by past and future changes in icean chemistry, Nat. Geosci., 2, 145–150, 2009.

Huber, M.: A hotter greenhouse?, Science, 231, 353–354, 2008.

Kelly, D. C.: Response of Antarctic (ODP Site 690) planktonic foraminifera to the Paleocene-Eocene thermal maximum: Faunal evidence for ocean/climate change, Paleoceanography, 17, 1071, doi:10.1029/2002PA000761, 2002.

Kelly, D. C., Bralower, T. J., and Zachos, J. C.: Evolutionary consequences of the latest Paleocene thermal maximum for tropical planktonic foraminifera, Palaeogeogr. Palaeocl., 141, 139–161, 1998.

Lourens, L. J., Sluijs, A., Kroon, D., Zachos, J. C., Thomas, E., Röhl, R., Bowles, J., and Raffi, I.: Astronomical pacing of late Paleocene to early Eocene global warming events, Nature, 435, 1083–1087, 2005.

McInerney, F. A. and Wing, S. L.: The Paleocene-Eocene Thermal Maximum: Perturbation of carbon cycle, climate, and biosphere with implications for the future, Annu. Rev. Earth Pl. Sc., 39, 489–516, 2011.

Murphy, B. H., Zachos, J. C., McCarren, H. K., Thomas, E., and Röhl, U.: High Resolution Records of the Elmo Event from Shatsky Rise, IODP Sites 1209 & 1211, Eos Trans. AGU,

BGD
9, 1237–1257, 2012

87, Fall Meet. Suppl., PP23C–1777, 2006.
Mutterlose, J., Linnert, C., and Norris, R.: Calcareous nannofossils from the Paleocene-Eocene Thermal Maximum of the equatorial Atlantic (ODP Site 1260B): Evidence for tropical warming, Mar. Micropaleontol., 65, 13–31, 2007.
Petrizzo, M. R.: The onset of the Paleocene-Eocene Thermal Maximum (PETM) at Sites 1209 and 1210 (Shatsky Rise, Pacific Ocean) as recorded by planktonic foraminifera, Mar. Micropaleontol., 63, 187–200, 2007.
Quillévéré, F., Norris, R. D., Kroon, D., and Wilson, P. A.: Transient ocean warming and shifts in carbon reservoirs during the early Danian, Earth Planet. Sc. Lett., 265, 600–615, 2008.
Ridgwell, A. and Schmidt, D. N.: Past constraints on the vulnerability of marine calcifiers to massive carbon dioxide release, Nat. Geosci., 3, 196–200, 2010.
Rohling, E. J. and Pälike, H.: Centennial-scale climate cooling with a sudden cold event around 8200 years ago, Nature, 434, 975–979, 2005.
Sexton, P. F., Norris, R. D., Wilson, P. A., Pälike, H., Westerhold, T., Röhl, U., Bolton, C. T., and Gibbs, S. J.: Eocene global warming events driven by ventilation of oceanic dissolved organic carbon, Nature, 471, 349–352, 2011.
Shipboard Scientific Party: Site 1209, in: Proc. ODP, Init. Repts., edited by: Bralower, T. J., Premoli Silva, I., Malone, M. J., Arthur, M. A., Averyt, K., Bown, P. R., Brassell, S. C., Channell, J. E. T., Clarke, L. J., Dutton, A., Eleson, J. W., Frank, T. D., Gylesjö, S., Hancock, H., Kano, H., Leckie, R. M., Marsaglia, K. M., McGuire, J., Moe, K. T., Petrizzo, M. R., Robinson, S. A., Röhl, U., Sager, W. W., Takeda, K., Thomas, D., Williams, T., and Zachos, J. C., 198, College Station, TX (Ocean Drilling Program), 1–102, doi:10.2973/odp.proc.ir.198.105.2002, 2002.
Sluijs, A. and Brinkhuis, H.: A dynamic climate and ecosystem state during the Paleocene-Eocene Thermal Maximum: inferences from dinoflagellate cyst assemblages on the New Jersey Shelf, Biogeosciences, 6, 1755–1781, doi:10.5194/bg-6-1755-2009, 2009.
Sluijs, A., Bowen, G. J., Brinkhuis, H., Lourens, L. J., and Thomas, E.: The Palaeocene-Eocene Thermal Maximum super greenhouse: biotic and geochemical signatures, age models and mechanisms of global change, in: Deep-Time Perspectives on Climate Change: Marrying the Signal from Computer Models and Biological Proxies, edited by: Williams, M., Haywood, A. M., Gregory, F. J., and Schmidt, D. N., The Micropaleontological Society, Geol. Soc. Sp., London, 323–349, 2007a.
Sluijs, A., Schouten, S., Pagani, M., Woltering, M., Brinkhuis, H., Sinninghe Damste, J. S., Dickens, G. R., Huber, M., Reichart, G.-J., Stein, R., Matthiessen, J., Lourens, L. J., Pe-

BGD
9, 1237–1257, 2012

dentchouk, N., Backman, J., Moran, K., & the Expedition 302 Scientists: Environmental precursors to rapid light carbon injection at the Paleocene/Eocene boundary, Nature, 450, 1218–1221, 2007b.

Sluijs, A., Röhl, U., Schouten, S., Brumsack, H.-J., Sangiorgi, F., Sinninghe Damste, J. S., and Brinkhuis, H.: Arctic late Paleocene-early Eocene paleoenvironments with special emphasis on the Paleocene-Eocene thermal maximum (Lomonosov Ridge, Integrated Ocean Drilling Program Expedition 302), Paleoceanography, 23, PA1S11, doi:10.1029/2007PA001495, 2008.

Sluijs, A., Schouten, S., Donders, T. H., Schoon, P. L., Röhl, U., Reichart, G.-J., Sangiorgi, F., Kim, J. H., Sinninghe Damsté, J. S., and Brinkhuis, H.: Warm and Wet Arctic Conditions during Eocene Thermal Maximum 2, Nat. Geosci., 2, 777–780, doi:10.1038/NGEO668, 2009.

Stap, L., Lourens, L. J., Thomas, E., Sluijs, A., Bohaty, S., and Zachos, J. C.: High resolution deep-sea carbon and oxygen isotope records of Eocene Thermal Maximum 2 and H2, Geology, 38, 607–610, 2010.

Thomas, D. J., Zachos, J. C., Bralower, T. J., Thomas, E., and Bohaty, S.: Warming the Fuel for the Fire: Evidence for the thermal dissociation of methane hydrate during the Paleocene-Eocene thermal maximum, Geology, 30, 1067–1070, 2002.

Wagner, D. H.: SiZer download page, available at: http://www.wagner.com/SiZer/SiZerDownload.html, last access: January 2012, 2009.

Westerhold, T. and Röhl, U.: Data report: revised composite depth records for Shatsky Rise Sites 1209, 1210, and 1211, Proc. Ocean Drill. Program, Sci. Results, 198, 1–26, doi:10.2973/odp.proc.sr.198.122.2006, 2006.

Zachos, J. C., Wara, M. W., Bohaty, S., Delaney, M. L., Petrizzo, M. R., Brill, A., Bralower, T. J., and Premoli-Silva, I.: A transient rise in tropical sea surface temperature during the Paleocene-Eocene Thermal Maximum, Science, 302, 1551–1554, 2003.

Zachos, J. C., Röhl, U., Schellenberg, S. A., Sluijs, A., Hodell, D. A., Kelly, D. C., Thomas, E., Nicolo, M., Raffi, I., Lourens, L. J., McCarren, H., Kroon, D.: Rapid Acidification of the Ocean During the Paleocene-Eocene Thermal Maximum, Science, 308, 1611–1615, 2005.

Zachos, J. C., McCarren, H., Murphy, B., Röhl, U., and Westerhold, T.: Tempo and scale of late Paleocene and early Eocene carbon isotope cycles: Implications for the origin of hyperthermals, Earth Planet. Sc. Lett., 299, 242–249, 2010.

Zeebe, R. E., Zachos, J. C., and Dickens, G. R.: Carbon dioxide forcing alone insufficient to explain Palaeocene-Eocene Thermal Maximum warming, Nat. Geosci., 2, 576–580, 2009.

BGD
9, 1237–1257, 2012

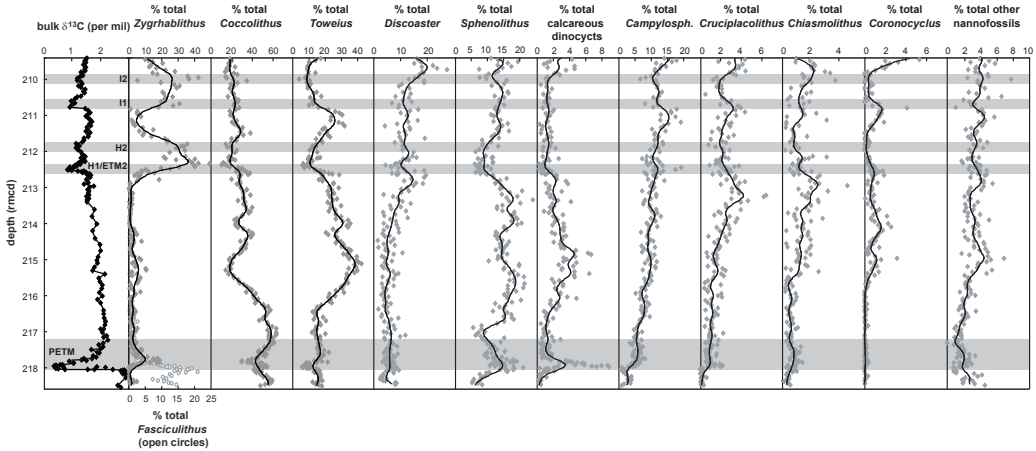

Fig. 1. Abundances of the most common taxa across the focal interval, illustrating raw percent data (grey diamonds) and the SiZer smoothed records (black lines), on a depth scale. In the first panel is the bulk carbonate carbon isotope record (Zachos et al., 2003; Murphy et al., 2006) with the CIE intervals highlighted in grey. *Campylosp.* – *Campylosphaera*. Depth – revised metres composite depth (rmcd, Westerhold and Röhl, 2006).

BGD
9, 1237–1257, 2012

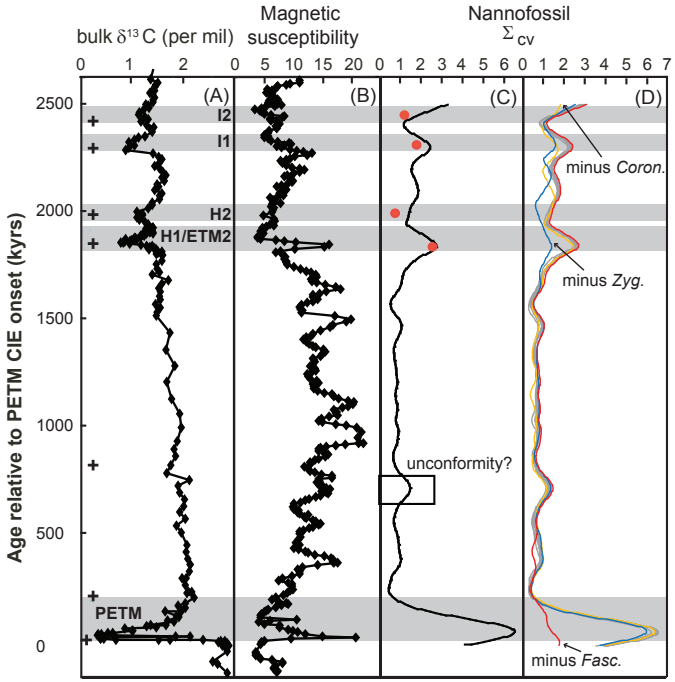

Fig. 2. Carbon isotope, magnetic susceptibility and calcareous nannofossil records from the Paleocene-Eocene interval at ODP Site 1209 against age relative to the PETM. In panel **(A)** is the bulk carbonate carbon isotope record (Zachos et al., 2003; Murphy et al., 2006), with the CIEs highlighted in grey and chronstratigraphic tie-points indicated by black crosses, and panel **(B)** shows the accompanying magnetic susceptibility record (Bralower et al., 2002). In panel **(C)** are summed coefficients of variation (Σ_{cv}) across age windows of 150 kyr (in black), with values calculated across the duration of each CIE smaller than 150 kyr indicated by red circles. In panel **(D)** is the Σ_{cv} record calculated excluding individual taxa. Only the records excluding *Coronocyclus* (yellow), *Zygrhablithus* (blue) and *Fasciculithus* (red) are indicated in color while the rest of the records that are virtually indistinguishable are shown in dark grey.

BGD
9, 1237–1257, 2012

Scaled biotic disruption during early Eocene global warming events

S. J. Gibbs et al.

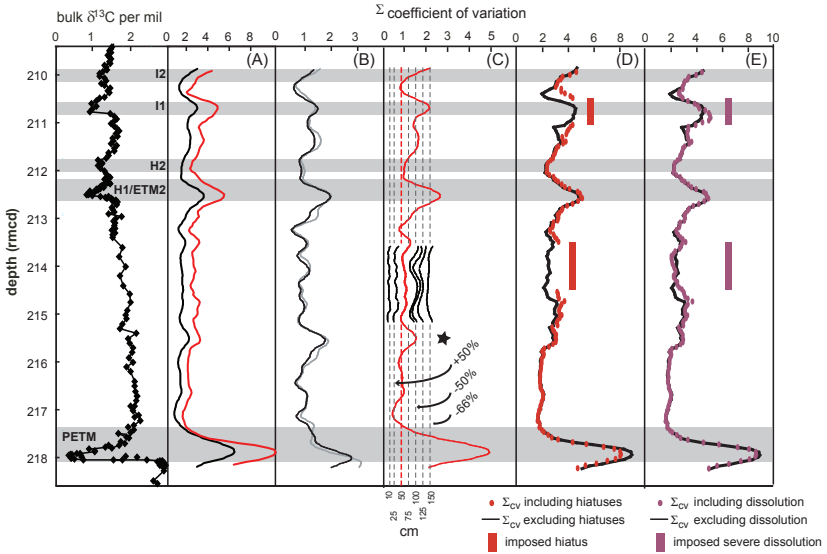

Fig. 3. Sensitivity tests and comparison of downcore summed coefficients of variation records. Σ_{cv} records in **(A)**, are generated from smoothed taxon records and from the raw data. In **(B)** is a comparison of total summed standard deviation of the smoothed data using standard deviations divided by the taxon's average across 50 cm (grey line) and across 100 cm windows (black line) compared with **(A)** where the standard deviations are divided by the taxon's average abundance across the entire interval. In **(C)** is a comparison of background Σ_{cv} values resulting from using different window sizes, extrapolated as vertical dashed lines with the 50 cm background Σ_{cv} level highlighted in red. Also marked is the sedimentation rate change equivalent (in percent) to which these background levels correspond. In panels **(D)** and **(E)** are the results of artificially introduced hiatuses and intervals of intense dissolution. The original Σ_{cv} record is shown in black and the records that include imposed hiatuses and dissolution are shown in red and purple, respectively. The intervals where hiatuses and dissolution have been introduced are highlighted by red and purple bars.

BGD
9, 1237–1257, 2012

Scaled biotic disruption during early Eocene global warming events

S. J. Gibbs et al.

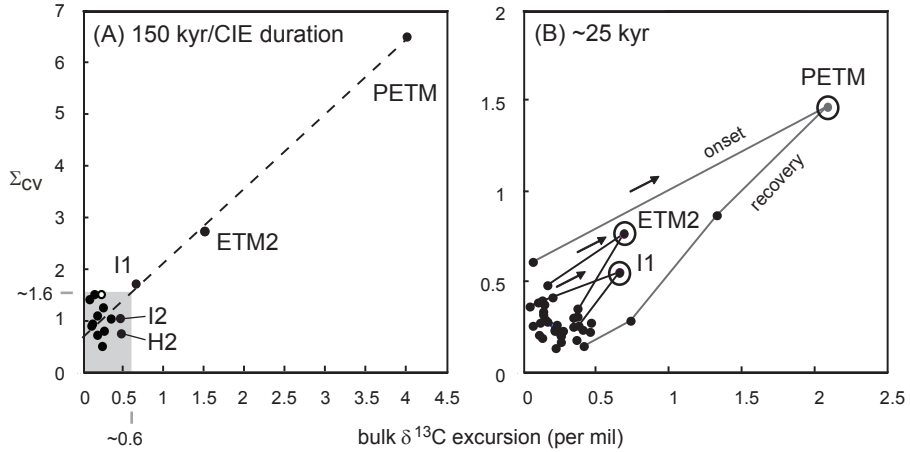

Fig. 4. Scatter plots of summed standard deviation (Σ_{cv}) against magnitude of carbon isotope excursion. In plot **(A)**, the Σ_{cv} values from Fig. 2c are plotted for each peak (using the values highlighted by red circles for H2, I1 and I2) and every intervening 150 kyr. The position of the Σ_{cv} datapoints for the PETM and ETM2 are shown against inferred maximum bulk carbonate $\delta^{13}C$ values (Lourens et al., 2005; Zachos et al., 2005). The level of a suspected unconformity at ~700 kyr above the PETM onset, is plotted as an open black circle and the grey area encompasses "background". In plot **(B)** are Σ_{cv} values across 25 kyr with values plotted for the peak excursions (open black circles) and every intervening 50 kyr. Only data that are spaced at least as widely apart as the standard deviation window are plotted in order for each datapoint to be independent of its neighbors. Stratigraphically adjacent data points are joined by line with the arrows indicating the up-section direction.

BGD
9, 1237–1257, 2012

Scaled biotic disruption during early Eocene global warming events

S. J. Gibbs et al.

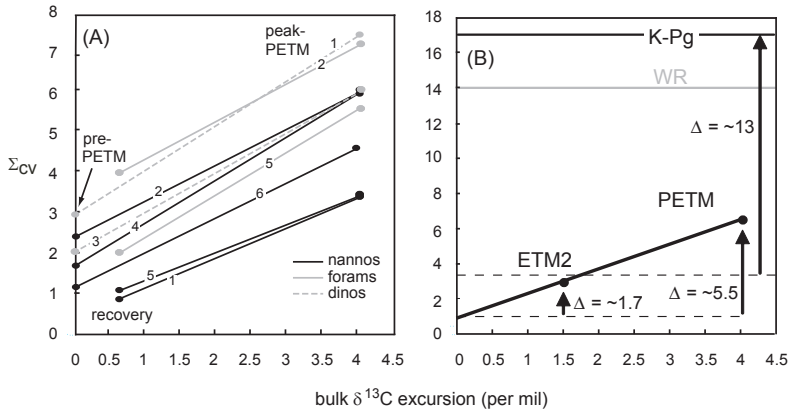

Fig. 5. Scatter plots of summed coefficients of variation (Σ_{cv}) against magnitude of CIE for multiple plankton groups and for comparison with the Cretaceous-Paleogene boundary mass extinction event. In plot **(A)** are background and peak PETM Σ_{cv} values for multiple PETM sites – nannofossils (black circles, black lines), planktonic foraminifera (grey circles, grey lines) and dinoflagellate cysts (grey circles, grey dashed lines). Where possible pre-event Σ_{cv} values are plotted but where missing then the Σ_{cv} values from the recovery interval are used. 1 – ODP onshore drill site Bass River [nannofossils (Gibbs et al., 2010) and dinocysts (Sluijs and Brinkhuis, 2009)]; 2 – ODP Site 690, Southern Ocean [nannofossils (Bralower, 2002) and planktonic foraminifera (Kelly, 2002)]; 3 – Lomonosov Ridge, Arctic Ocean [dinocysts (Sluijs et al., 2008)]; 4 – TDP, Tanzanian drilling project site 14 [nannofossils (Bown and Pearson, 2009)]; 5 – ODP Site 1209 [nannofossils – herein – and planktonic foraminifera (Petrizzo, 2007)]; 6 – ODP Site 1260, Demerara Rise, Atlantic Ocean [nannofossils (Mutterlose et al., 2007)]. All Σ_{cv} data use 10 taxa for comparison or, for the foraminifera data, normalized to 10 taxa. Plot **(B)** illustrates the $\Delta\Sigma_{cv}$ of the PETM and ETM2 from Site 1209 compared with the K-Pg using data from Site 1210 [horizontal black line (Bown, 2005)] and Site 1262 [WR – Walvis Ridge, horizontal grey line (Bernaola and Monechi, 2007)]. The K-Pg Σ_{cv} value is not plotted against its respective $\delta^{13}C$ value as this is not a meaningful measure of environmental perturbation for this event.

BGD
9, 1237–1257, 2012

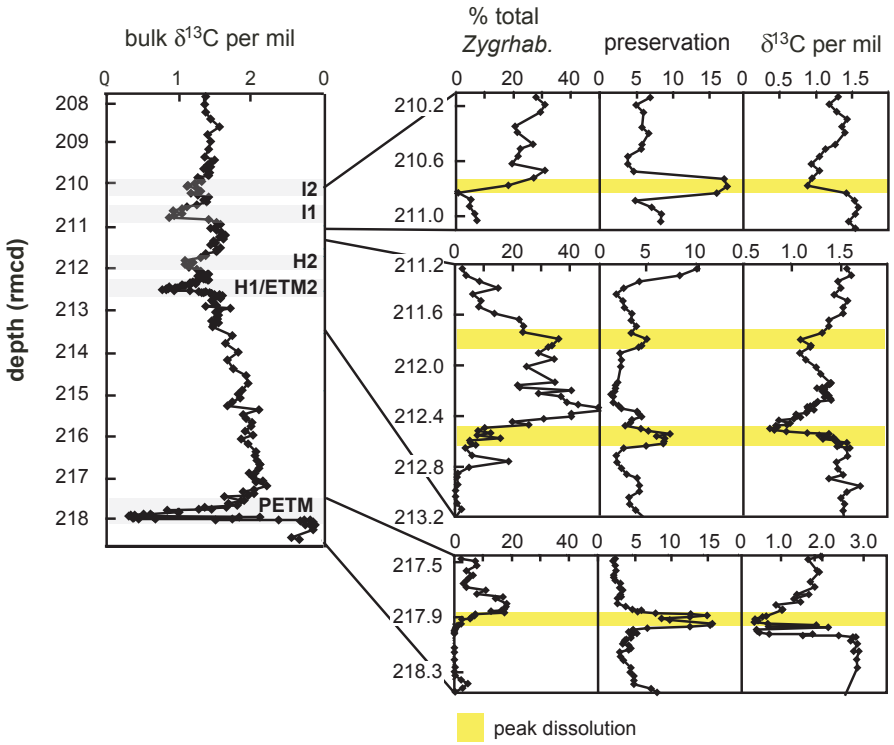

Fig. 6. Relationships between dissolution, the CIEs and the abundance of *Zygrhablithus*. The nannofossil-based preservation index uses the ratio of indeterminate *Toweius* to identifiable *Toweius* (Gibbs et al., 2006b, 2010). The peak in *Zygrhablithus* associated with each CIE occurs at the start of the carbon isotope recovery in each case and is consistently above the level of peak dissolution (highlighted in yellow).

BGD
9, 1237–1257, 2012